Check for updates

physica status solidi rrl
www.pss-rapid.com

# Ultrathin $Al_{1-x}Sc_xN$ for Low-Voltage-Driven Ferroelectric-Based Devices

*Georg Schönweger,* Md Redwanul Islam, Niklas Wolff, Adrian Petraru, Lorenz Kienle, Hermann Kohlstedt, and Simon Fichtner**

**Thickness scaling of ferroelectricity in $Al_{1-x}Sc_xN$ is a determining factor for its potential application in neuromorphic computing and memory devices. In this letter, ultrathin (10 nm) $Al_{0.72}Sc_{0.28}N$ films that are ferroelectrically switchable at room temperature are reported on. All-epitaxial $Al_{0.72}Sc_{0.28}N$/Pt heterostructures are grown by magnetron sputtering onto GaN/sapphire substrates followed by an in situ Pt capping approach to avoid oxidation of the $Al_{0.72}Sc_{0.28}N$ film surface. Structural characterization by X-Ray diffraction and transmission electron microscopy reveals the established epitaxy. The thus-obtained high-quality films in combination with in situ capping facilitate ferroelectric switching of $Al_{1-x}Sc_xN$ in the ultrathin regime. The analysis of the relative permittivity and coercive field dependence on $Al_{0.72}Sc_{0.28}N$ film thicknesses in the range from 100 nm down to 10 nm indicates only moderate scaling effects, suggesting that the critical thickness for ferroelectricity is not yet approached. Furthermore, the deposited layer stack demonstrates the possibility of including ultrathin ferroelectric $Al_{1-x}Sc_xN$ into all-epitaxial GaN-based devices using sputter deposition techniques. Thus, the integration and scaling potential of all-epitaxial ultrathin $Al_{1-x}Sc_xN$ offering high storage density paired with low-voltage operation desired for state-of-the-art ferroelectric memory devices are highlighted.**

## 1. Introduction

The high coercive field ($E_c$) and the high, stable remanent polarization separate the ferroelectric properties recently discovered in materials with wurtzite-type structure from classical ferroelectrics.[1–4] This raises hopes for particularly good scalability of wurtzite-type-based ferroelectric devices. In addition, the complementary metal-oxide semiconductor compatibility and the well-established industrial deposition process make $Al_{1-x}Sc_xN$ thin films highly attractive for building novel neuromorphic computing and memory devices such as ferroelectric field-effect transistors (FeFET) and ferroelectric tunnel junctions (FTJs).[5–9] Furthermore, it is expected that wurtzite-type ferroelectrics such as $Al_{1-x}Sc_xN$ introduce ferroelectricity into III-N technology, resulting in a straightforward approach to realize, for example, GaN-embedded memory. Such ferroelectric all-epitaxial all-wurtzite type $Al_{1-x}Sc_xN$/GaN heterostructures were demonstrated recently.[10,11] However, a very low film thickness of the ferroelectric layer is needed for following the general trend of miniaturization and increasing storage density in all of the aforementioned devices. In this context, $Al_{1-x}Sc_xN$ offers high scalability due to its high $E_c$, making it possible to tailor the film thickness to the ultrathin regime to achieve reasonable memory windows and low operating voltages.[12] Furthermore, in terms of device design, ultrathin ferroelectric films are a prerequisite for building FTJs.[7] Reducing the thickness to the ultrathin regime (<30 nm) is often accompanied by a material-specific diminution of remanent polarization ($P_r$), a drastic increase of $E_c$, or results in a total loss of ferroelectricity.[13–15] To our best knowledge, up to now, no thickness scaling study on ferroelectric epitaxial $Al_{1-x}Sc_xN$ heterostructures was conducted. Also for nonepitaxial heterostructures, only a small number of studies were performed. Below 20 nm film thickness, measurements that suggest ferroelectricity at elevated temperatures or indirectly through scanning nonlinear dielectric microscopy are accessible.[16,17] Very recently, partly ferroelectric switching of ≈12 nm-thick $Al_{1-x}Sc_xN$ was reported by performing positive-up-negative-down (PUND) measurements at room temperature.[18] The availability of ferroelectric sub-20 nm films is however crucial in order to reach switching voltages in the low-single-digit volt range that is desired for advanced circuits as

G. Schönweger, A. Petraru, H. Kohlstedt
Institute of Electrical and Information Engineering
Christian-Albrechts-Universität zu Kiel
Kaiserstrasse 2, 24143 Kiel, Germany
E-mail: gmsc@tf.uni-kiel.de

M. R. Islam, N. Wolff, L. Kienle, S. Fichtner
Institute for Material Science
Christian-Albrechts-Universität zu Kiel
Kaiserstrasse 2, 24143 Kiel, Germany
E-mail: sif@tf.uni-kiel.de

G. Schönweger, S. Fichtner
Fraunhofer Institute for Silicon Technology (ISIT)
Fraunhoferstr. 1, D-25524 Itzehoe, Germany

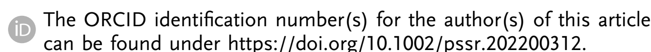
The ORCID identification number(s) for the author(s) of this article can be found under https://doi.org/10.1002/pssr.202200312.

© 2022 The Authors. physica status solidi (RRL) Rapid Research Letters published by Wiley-VCH GmbH. This is an open access article under the terms of the Creative Commons Attribution License, which permits use, distribution and reproduction in any medium, provided the original work is properly cited.

**DOI: 10.1002/pssr.202200312**


© 2022 The Authors. physica status solidi (RRL) Rapid Research Letters published by Wiley-VCH GmbH

well as sufficiently small line widths for large-scale integration. Here we present our recent results on the thickness scaling (from 100 nm down to 10 nm) of epitaxial $Al_{0.72}Sc_{0.28}N$ grown on epitaxial Pt via sputter deposition on GaN/sapphire substrates. This epitaxial growth enables significantly better crystal properties of $Al_{1-x}Sc_xN$ compared with previous studies on materials with cylindrical symmetry.[11,16,17,19] In addition, as reported in several studies, epitaxial growth of $Al_{1-x}Sc_xN$ induced an improved coupling coefficient and quality factor in resonators as well as a reduction of the coercive field due to strain effects.[11,20–22] In our study, the low root mean square (RMS) roughness (see Figure S1, Supporting Information) and the sharp interfaces combined with an in situ Pt capping result in an improved ferroelectric response. Consequently, we were able to record typical butterfly-shaped capacitance–voltage ($C$–$U$) loops as well as current density over the electric field ($J$–$E$) loops at room temperature, demonstrating clearly distinguishable ferroelectric switching down to 10 nm film thickness. Therefore, the general feasibility of ultrathin $Al_{1-x}Sc_xN$ for future device integration and low voltage operation is demonstrated. In addition, this integration of epitaxial ultrathin ferroelectric $Al_{1-x}Sc_xN$ into a III-N heterostructure further highlights the viability of introducing new functionality into III-N-based devices.

## 2. Device Fabrication and Characterization Methods

All films were grown by sputter deposition in an Oerlikon (now Evatec) MSQ 200 multisource system on top of commercially available GaN/sapphire substrates. A 12 nm-thick epitaxial Pt layer (bottom electrode) was DC-sputtered at 500 °C and 600 W under Krypton atmosphere at a deposition pressure of $5.4 \times 10^{-3}$ mbar. The base pressure was below $5 \times 10^{-7}$ mbar. The X-ray diffraction (XRD) measurements were carried out using monochromatic $K_\alpha$ radiation in a Seifert XRD 3000 PTS system ($\theta$–$2\theta$ scan) as well as in a Rigaku SmartLab diffractometer (in-plane phi-scan, $\theta$–$2\theta$ scan, rocking curve). The $Al_{0.72}Sc_{0.28}N$ thin films were grown by pulsed DC cosputtering at 450 °C. Details about the process can be found in other studies.[23,24] The 10- and 20 nm-thick $Al_{0.72}Sc_{0.28}N$ layers were capped in situ with 100 nm-thick Pt, while 50 and 100 nm were capped after vacuum break. The in situ Pt top electrode was deposited at 450 °C and 400 W under Krypton atmosphere at a deposition pressure of $6.7 \times 10^{-3}$ mbar after reaching a base pressure of $5 \times 10^{-7}$ mbar. Square top electrodes were structured via lithography and ion-beam etching (IBE, Oxford Instruments Ionfab 300). Dry etching stopped abruptly after detecting Sc via a secondary-ion mass spectrometer (SIMS), thus not etching through the $Al_{0.72}Sc_{0.28}N$ layer. Capacitance measurements were performed on a Hewlett Packard 4284 A Precision LCR meter. High-frequency $J$–$E$ loops were measured using an AixACCT TF Analyzer 3000. A cross-section specimen of the in situ-capped 10 nm-thick $Al_{0.72}Sc_{0.28}N$ sample was prepared using a standard focused ion beam (FIB) procedure and analyzed using high-resolution transmission electron microscopy (HRTEM, Tecnai F30, operated at 300 kV, field emission gun) and fast Fourier-transform (FFT) patterns.

## 3. Results and Discussions

The current response depending on the applied electric field for capacitors with various $Al_{0.72}Sc_{0.28}N$ film thicknesses is depicted in **Figure 1**a. Ferroelectric switching peaks appear for film thicknesses down to 10 nm. Leakage currents commonly present in thin $Al_{1-x}Sc_xN$ films are emerging also in our all-epitaxial heterostructures.[17,19,25] In this context, a comparably low tan $\delta$ for the respective film thickness was found to be crucial to ferroelectrically switch films below 20 nm film thickness before electrical breakdown occurs.

Noticeably, with decreasing film thickness, an increase in the area of the current peaks in the $J-E$ loops as well as an increase in the total area of the dynamic leakage current compensated (DLCC) $P-E$ loops (Figure S2, Supporting Information) are visible.[26] However, as discussed in the Supporting information, the corrected $P-E$ loops of the ultrathin films are not fully leakage compensated, leading to unrealistically high $P_r$ values. Thus, the apparent increase in $P_r$ with decreasing film thickness could be due to a dynamic leakage contribution which is closely correlated to the switching event.

The coercive field slightly increases with decreasing film thickness. Therefore, especially for ultrathin films, we had to increase the maximum electric field applied. This goes hand in hand with an increase in the leakage currents as well as an

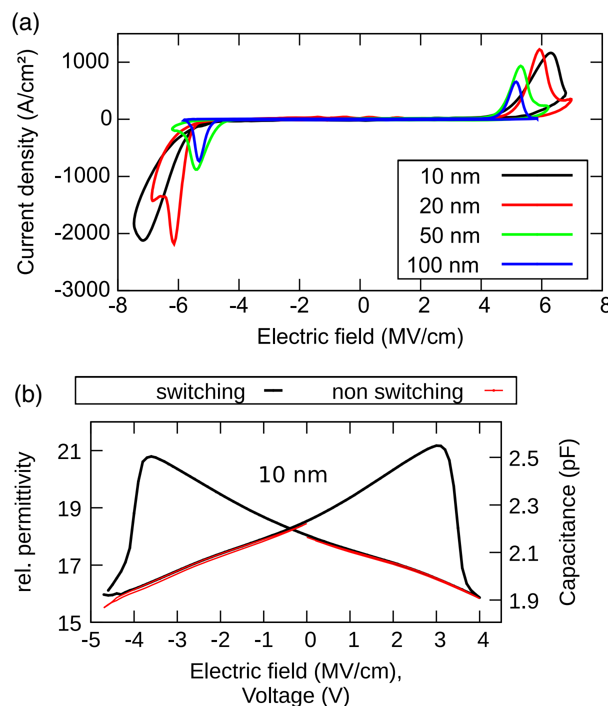


**Figure 1.** a) $J$–$E$ loops of Pt(100 nm)/$Al_{0.72}Sc_{0.28}N$/Pt(12 nm) capacitors deposited on GaN/sapphire templates with varying $Al_{0.72}Sc_{0.28}N$ film thickness. All loops were measured at 80 kHz on $10 \times 10\,\mu m^2$ pads. b) Relative permittivity and capacitance as a function of the applied voltage and electric field for 10 nm-thick $Al_{0.72}Sc_{0.28}N$. The nonswitching half loops (red) were recorded by previously switching the capacitor to the respective polarity. Measured on $10 \times 10\,\mu m^2$ pads with a small signal of 0.1 $V_{pp}$ at 100 kHz swept in 0.1 V steps with a delay of 300 ms per step.



© 2022 The Authors. physica status solidi (RRL) Rapid Research Letters published by Wiley-VCH GmbH

18626270, 2023, 1, Downloaded from https://onlinelibrary.wiley.com/doi/10.1002/pssr.202200312 by Readcube (Labtiva Inc.), Wiley Online Library on [05/07/2023]. See the Terms and Conditions (https://onlinelibrary.wiley.com/terms-and-conditions) on Wiley Online Library for rules of use; OA articles are governed by the applicable Creative Commons License

asymmetry in the current response, making it hard to identify clearly the switching peak at negative fields for the 10 nm-thick $Al_{0.72}Sc_{0.28}N$ film. However, the as-deposited polarization state of our films is nitrogen (N)-polar.[1] Consequently, ferroelectric switching at positive fields (from metal (M)-polar to N-polar) can only result after prior switching from N-Polarity to M-polarity at negative fields.

To further confirm ferroelectric switching of 10 nm-thick $Al_{0.72}Sc_{0.28}N$, *C–U* loops were recorded and are depicted in Figure 1b. The butterfly-shaped curve (black) demonstrates distinguishable ferroelectric switching.

In addition, nonswitching half loops (red) were recorded by measuring twice with the same polarity. No hysteretic behavior is observed for the nonswitching half-loops, thus giving additional evidence that the butterfly-shaped hysteresis for the switching loop originates from true ferroelectric switching. Previously, the coercive field in $Al_{1-x}Sc_xN$ thin films was observed to be almost independent of thickness for films thicker than ≈20 nm.[16,17,25] Similarly, in this study, $E_c$ determined via *C–U* as well as via *J–E* loops, as depicted in **Figure 2**, does not change considerably when decreasing the film thickness from 100 to 50 nm. When decreasing the film thickness further to 20 nm and especially to 10 nm, a moderate increase of the coercive field by about 25% is observed. The difference in the coercive field determined via *C–V* and *J–E* curves for the respective thickness is a result of the frequency dependence of $E_c$. In *C–V* loops the electric field is swept very slowly (≈20 mHz), while in *J–E* loops the measurement frequency is much higher (80 kHz).

The coercive field scaling in $Al_{1-x}Sc_xN$ is in strong contrast to classical ferroelectrics, as illustrated in **Figure 3**. In the perovskites (e.g., $BaTiO_3$, $SrBi_2Ta_2O_9$, PZT) $E_c$ is generally proportional to $d^{-2/3}$, according to the domain nucleation model elaborated from Kay–Dunn.[27] Dawber et al. included

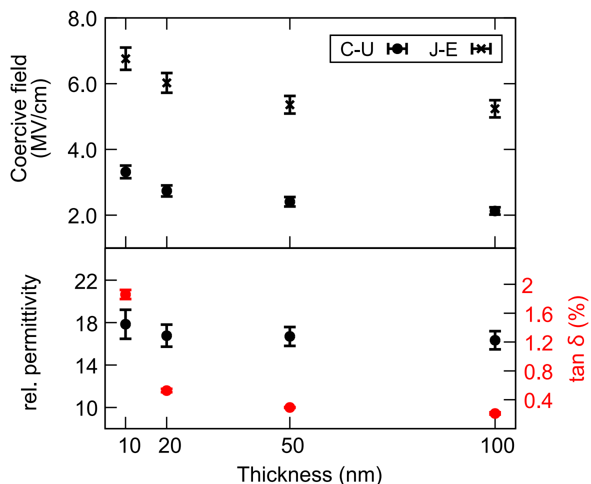


**Figure 2.** $E_c$, $\varepsilon_r$, and the loss tangent (tan $\delta$) depending on $Al_{0.72}Sc_{0.28}N$ film thickness. $\varepsilon_r$ and tan $\delta$ were measured at 100 kHz and 100 mV at 0 V bias. $E_c$ was determined via measuring *C–U* loops, keeping the time for a full sweep constant for the various film thicknesses as well as via *J–E* using a sinus signal at 80 kHz. The error bars for $E_c$ and $\varepsilon_r$ were calculated using an estimated capacitor side-length error of 0.4 µm and an estimated thickness error of 5%. In addition, for $E_c$ determination via *C–U* loops, the step width of the respective voltage sweep was included in the error calculation.

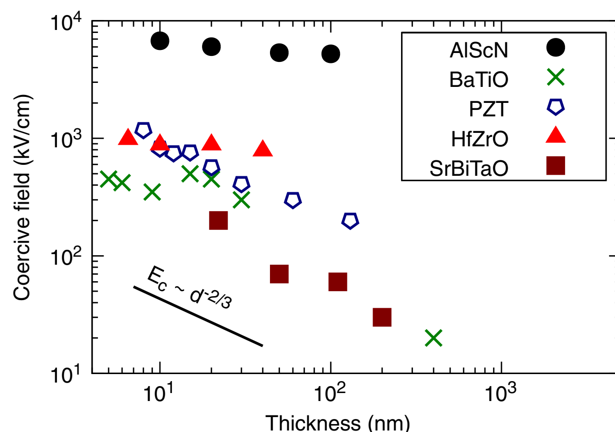


**Figure 3.** Coercive field scaling of PZT,[14,29–32] $BaTiO_3$, $SrBi_2Ta_2O_9$, Zr-doped $HfO_2$,[33] and of our $Al_{0.72}Sc_{0.28}N$ films.

contributions from the depolarization field due to incomplete screening at the electrodes to the Kay–Dunn model, being in good agreement with experimental data of ultrathin films.[28]

However, both models are apparently not able to describe the scaling behavior of the relatively new ferroelectrics $HfO_2$ and $Al_{1-x}Sc_xN$. For $HfO_2$, the nonscaling of $E_c$ is explained by nanometer-scale confinement of the ferroelectric domains due to the grain-like multiphase structure, which is independent of film thickness.[33] Although the wurtzite phase of $Al_{1-x}Sc_xN$ is very stable and thus only one phase exists, a different domain shape as assumed by Kay and Dunn could explain the deviations from the classical $E_c$ scaling. However, a low to moderate increase of $E_c$ with decreasing film thickness is observed in our films and was reported recently also in other studies. For nonepitaxial films, this was attributed to a change of *c*-to-*a* lattice parameter ratio with decreasing $Al_{1-x}Sc_xN$ film thickness.[18] As a consequence, the internal parameter *u* decreased, which is known to result in an increase of the coercive field.[11] However, XRD measurements (not shown here) of our films reveal no scaling of *u*. Very recently the low $E_c$ scaling of nonepitaxial $Al_{1-x}Sc_xN$ down to 20 nm film thickness was related to charge-injection effects through a very thin interfacial dielectric layer.[34,35] The lowering of $E_c$ due to in situ capping of ultrathin films, as depicted in Figure S3, Supporting Information, supports this explanation. In addition, the prevention of an oxide layer formation in ultrathin films results in a lowering of the leakage currents, highlighting the improved ferroelectric response due to in situ Pt capping.

For Zr-doped $HfO_2$, a lower thickness limit for ferroelectricity of 5 nm was found and attributed to the formation of a dead layer if deposited on TiN or W bottom electrodes, while on a Pt bottom electrode, the dead layer formation could be suppressed and ferroelectric switching was demonstrated down to 2.5 nm thickness.[36] On the other hand, when $HfO_2$-based ferroelectrics become thicker (>≈50 nm), ferroelectricity becomes unstable due to the energetically more favourable paraelectric phase.[33] In general, the dramatic degradation or total loss of ferroelectric properties in ultrathin films due to such a nonswitching interfacial layer (dead layer[37]) is typically accompanied by a decrease of $\varepsilon_r$.[14,36,38] The moderate scaling


© 2022 The Authors. physica status solidi (RRL) Rapid Research Letters published by Wiley-VCH GmbH

18626270, 2023, 1, Downloaded from https://onlinelibrary.wiley.com/doi/10.1002/pssr.202200312 by Readcube (Labtiva Inc.), Wiley Online Library on [05/07/2023]. See the Terms and Conditions (https://onlinelibrary.wiley.com/terms-and-conditions) on Wiley Online Library for rules of use; OA articles are governed by the applicable Creative Commons License

of $E_c$ and nonscaling of $\varepsilon_r$ with thickness leads to our conclusion that the lower thickness limit in $Al_{1-x}Sc_xN$ is not yet approached at 10 nm, and stable ferroelectricity can be expected also for films <10 nm thickness. This highlights the thickness scalability of ferroelectric $Al_{1-x}Sc_xN$, ranging from at least 600 nm down to the single-digit nanometer range.[1]

Since, together with in situ capping, the bottom Pt interface can be considered crucial in order to obtain ferroelectric $Al_{1-x}Sc_xN$ films with very low thicknesses, we confirmed that our epitaxial electrodes are of significantly better texture than what can be expected of Pt films grown nonepitaxially over, for example, c-Si.[19,39] The structure of Pt grown on GaN/sapphire templates is revealed via the $\theta$–$2\theta$ scan depicted in **Figure 4**a. The expected out-of-plane 111 orientation for Pt and 0002 orientation for GaN is visible. Laue oscillations, which are sensitive to crystalline disorder, appear for the Pt 111 reflection.[40]

The thus expected high crystallinity is confirmed by rocking curve (RC) measurements (not shown here) of the 111 Pt reflection; the full-width at half-maximum (FWHM) of 0.1° is indicative of a strain and defect-poor crystalline phase with high out-of-plane orientation. Furthermore, the distinct Laue oscillations allow for determining the thickness ($t$) of the ordered crystal volume.[40]

$$t = \frac{3\lambda}{2(\sin\theta_1 - \sin\theta_{-1})} \quad (1)$$

Using Equation (1), with $\theta_1$ and $\theta_{-1}$ corresponding to the maximum of the peaks right and left from the center of the Pt 111 reflection, an average film thickness of 11 nm is determined.

The in-plane ordering was resolved by recording a phi-scan of the nonspecular 131 Pt reflection as well as the nonspecular 01–10 $Al_{0.72}Sc_{0.28}N$ reflection, as depicted in Figure 4b. A sixfold symmetry is visible, evidencing epitaxial (in-plane ordered) growth. The expected 0002 orientation of 10 nm-thick $Al_{0.72}Sc_{0.28}N$ grown on epitaxial Pt is revealed by the $\theta$–$2\theta$ scan depicted in Figure 4c.

The intensity profile across the HRTEM micrograph of the Pt(100 nm)/$Al_{0.72}Sc_{0.28}N$(10 nm)/Pt(12 nm)/GaN/sapphire heterostructure is shown in **Figure 5** and film thicknesses of 10 nm for $Al_{0.72}Sc_{0.28}N$ and 12 nm for Pt are determined on local average. The latter is in excellent agreement with the Pt thickness calculated using Equation (1). The blurred interfaces present in the HRTEM image are attributed to the finite roughness of the heterostructure. The FFT pattern clearly reveals an epitaxial growth for both layers.

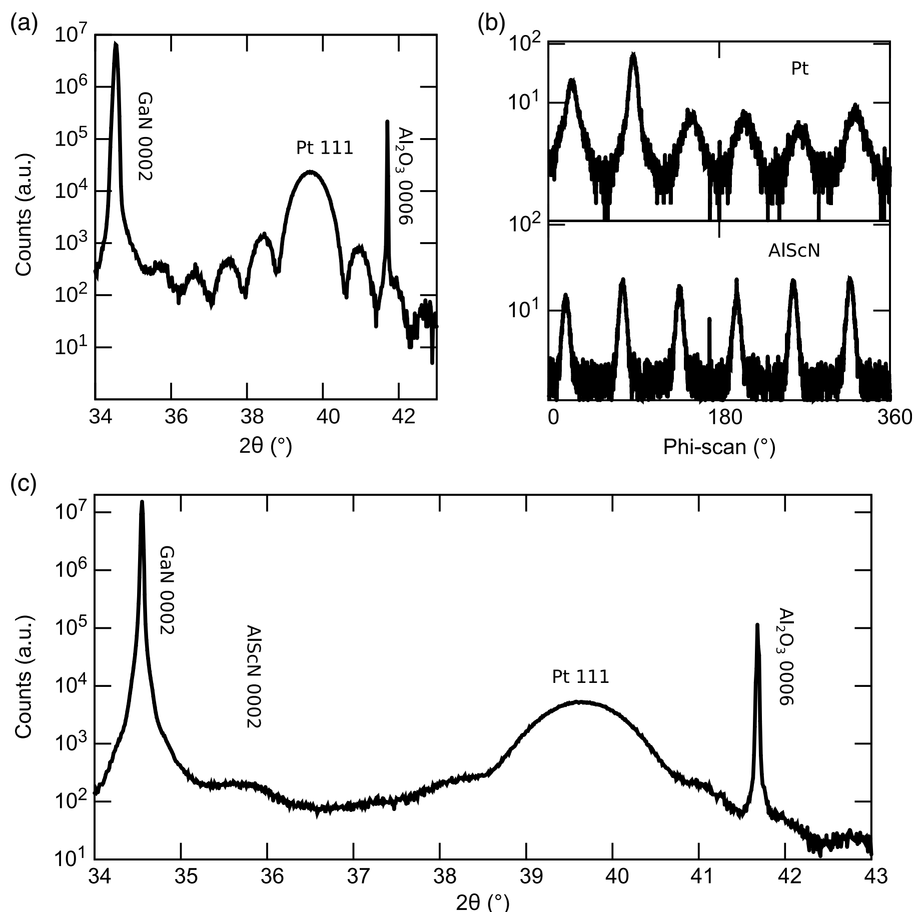


**Figure 4.** a) $\theta$–$2\theta$ scan and b) (top) smoothed phi-scan for the nonspecular Pt 131 reflection of 12 nm Pt on GaN/sapphire as well as (bottom) smoothed phi-scan for the nonspecular $Al_{0.72}Sc_{0.28}N$ 01–10 reflection of 20 nm $Al_{0.72}Sc_{0.28}N$ on Pt(12 nm)/GaN/sapphire. c) $\theta$–$2\theta$ scan of the film shown in (a) after deposition of 10 nm $Al_{0.72}Sc_{0.28}N$ followed by 5 nm in situ capping with Pt.


© 2022 The Authors. physica status solidi (RRL) Rapid Research Letters published by Wiley-VCH GmbH
18626270, 2023, 1, Downloaded from https://onlinelibrary.wiley.com/doi/10.1002/pssr.202200312 by Readcube (Labtiva Inc.), Wiley Online Library on [05/07/2023]. See the Terms and Conditions (https://onlinelibrary.wiley.com/terms-and-conditions) on Wiley Online Library for rules of use; OA articles are governed by the applicable Creative Commons License

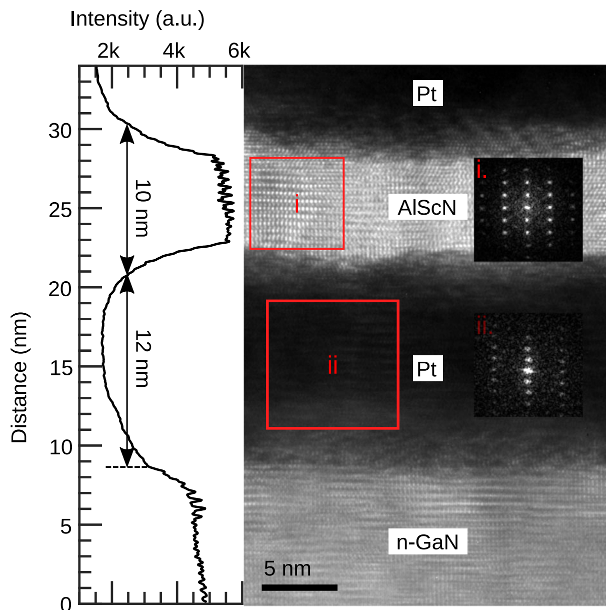


**Figure 5.** HRTEM image (right) and corresponding average thickness profile (left) of the Pt(100 nm)/$Al_{0.72}Sc_{0.28}N$(10 nm)/Pt(12 nm)/GaN/sapphire heterostructure. In the inset, the FFT pattern for i) $Al_{0.72}Sc_{0.28}N$ and ii) Pt is depicted.

The FWHM of the $Al_{1-x}Sc_xN$ 0002 RC decreases with decreasing film thickness, as illustrated in Figure S4, Supporting Information. This is in strong contrast to films grown on nonepitaxial Pt, where an increase of the RC with decreasing film thickness is observed.[16] Therefore, the crystal quality of the first few nanometers of $Al_{1-x}Sc_xN$ grown on epitaxial Pt is considerably higher than if grown on nonepitaxial Pt. Thus, the epitaxial growth in combination with the in situ capping of $Al_{1-x}Sc_xN$ to avoid oxidation has a significant impact on the ferroelectric switching behavior, especially for ultrathin films.

## 4. Conclusion

Distinguishable ferroelectric switching of 10 nm-thick $Al_{0.72}Sc_{0.28}N$ was demonstrated at room temperature. Only low-to-moderate changes in the coercive field and constant $\varepsilon_r$ for films ranging from 100 nm down to 10 nm thickness were confirmed. Thus, no indications of instabilities of the ferroelectric phase or considerable contributions from dead layers are present. Therefore, it is expected that further potential remains to scale ferroelectric $Al_{1-x}Sc_xN$ to even lower thicknesses. This constitutes an important step toward integrated ferroelectric wurtzite-type thin films with low single-digit switching voltages. Thus, our results highlight the general feasibility of using $Al_{1-x}Sc_xN$ as an active layer for integrated electronic devices with low operating voltage and high storage density. Furthermore, the all-epitaxial growth on GaN/sapphire and the thus-obtained high-quality film and interfaces not only improve the ferroelectric response in the ultrathin regime but also make $Al_{1-x}Sc_xN$ highly attractive for the integration of ferroelectric functionality into all-epitaxial III-N devices.

## Supporting Information

Supporting Information is available from the Wiley Online Library or from the author.

## Acknowledgements

This work was supported by the project "ForMikro-SALSA" (grant no. 16ES1053) from the Federal Ministry of Education and Research (BMBF) and the Deutsche Forschungsgemeinschaft (DFG) under the scheme of the collaborative research centers (CRC) 1261 and 1461. [Correction added after publication 05 January 2023: the affiliations were updated.]

Open Access funding enabled and organized by Projekt DEAL.

## Conflict of Interest

The authors declare no conflict of interest.

## Data Availability Statement

The data that support the findings of this study are available from the corresponding author upon reasonable request.

## Keywords

aluminum–scandium–nitride ($Al_{1-x}Sc_xN$), epitaxial growth, ferroelectrics, gallium nitride, ultrathin

Received: August 23, 2022
Revised: September 19, 2022
Published online: October 12, 2022

[1] S. Fichtner, N. Wolff, F. Lofink, L. Kienle, B. Wagner, *J. Appl. Phys.* **2019**, *125*, 114103.
[2] K. Ferri, S. Bachu, W. Zhu, M. Imperatore, J. Hayden, N. Alem, N. Giebink, S. Trolier-McKinstry, J.-P. Maria, *J. Appl. Phys.* **2021**, *130*, 044101.
[3] J. Hayden, M. D. Hossain, Y. Xiong, K. Ferri, W. Zhu, M. V. Imperatore, N. Giebink, S. Trolier-McKinstry, I. Dabo, J.-P. Maria, *Phys. Rev. Mater.* **2021**, *5*, 044412.
[4] D. Wang, P. Wang, B. Wang, Z. Mi, *Appl. Phys. Lett.* **2021**, *119*, 111902.
[5] H. Mulaosmanovic, T. Mikolajick, S. Slesazeck, in *Topics in Applied Physics*, Springer, Singapore **2020**, pp. 399–411.
[6] T. Schenk, M. Pešić, S. Slesazeck, U. Schroeder, T. Mikolajick, *Rep. Progr. Phys.* **2020**, *83*, 086501.
[7] E. Y. Tsymbal, H. Kohlstedt, *Science* **2006**, *313*, 181.
[8] H. Kohlstedt, N. A. Pertsev, J. R. Contreras, R. Waser, *Phys. Rev. B* **2005**, *72*, 125341.
[9] X. Liu, D. Wang, J. Zheng, P. Musavigharavi, J. Miao, E. A. Stach, R. H. Olsson, D. Jariwala, *Nano Lett.* **2021**, *21*, 3753.
[10] P. Wang, D. Wang, N. M. Vu, T. Chiang, J. T. Heron, Z. Mi, *Appl. Phys. Lett.* **2021**, *118*, 223504.
[11] G. Schönweger, A. Petraru, M. R. Islam, N. Wolff, B. Haas, A. Hammud, C. Koch, L. Kienle, H. Kohlstedt, S. Fichtner, *Adv. Funct. Mater.* **2022**, *32*, 2109632.
[12] H. Mulaosmanovic, E. T. Breyer, T. Mikolajick, S. Slesazeck, *IEEE Trans. Electron Devices* **2019**, *66*, 3828.


© 2022 The Authors. physica status solidi (RRL) Rapid Research Letters published by Wiley-VCH GmbH

18626270, 2023, 1, Downloaded from https://onlinelibrary.wiley.com/doi/10.1002/pssr.202200312 by Readcube (Labtiva Inc.), Wiley Online Library on [05/07/2023]. See the Terms and Conditions (https://onlinelibrary.wiley.com/terms-and-conditions) on Wiley Online Library for rules of use; OA articles are governed by the applicable Creative Commons License

[13] H. Qiao, C. Wang, W. S. Choi, M. H. Park, Y. Kim, *Mater. Sci. Eng.: R: Rep.* **2021**, *145*, 100622.
[14] N. A. Pertsev, J. R. Contreras, V. G. Kukhar, B. Hermanns, H. Kohlstedt, R. Waser, *Appl. Phys. Lett.* **2003**, *83*, 3356.
[15] P. Chandra, M. Dawber, P. B. Littlewood, J. F. Scott, *Ferroelectrics* **2004**, *313*, 7.
[16] S. Yasuoka, T. Shimizu, A. Tateyama, M. Uehara, H. Yamada, M. Akiyama, Y. Hiranaga, Y. Cho, H. Funakubo, *J. Appl. Phys.* **2020**, *128*, 114103.
[17] R. Mizutani, S. Yasuoka, T. Shiraishi, T. Shimizu, M. Uehara, H. Yamada, M. Akiyama, O. Sakata, H. Funakubo, *Appl. Phys. Express* **2021**, *14*, 105501.
[18] S. Yasuoka, R. Mizutani, R. Ota, T. Shiraishi, T. Shimizu, S. Yasui, Y. Ehara, K. Nishida, M. Uehara, H. Yamada, M. Akiyama, Y. Imai, O. Sakata, H. Funakubo, *J. Ceram. Soc. Jpn.* **2022**, *130*, 436.
[19] D. Wang, J. Zheng, P. Musavigharavi, W. Zhu, A. C. Foucher, S. E. Trolier-McKinstry, E. A. Stach, R. H. Olsson, *IEEE Electron Device Lett.* **2020**, *41*, 1774.
[20] K. Yazawa, D. Drury, A. Zakutayev, G. L. Brennecka, *Appl. Phys. Lett.* **2021**, *118*, 162903.
[21] G. Wingqvist, F. Tasnádi, A. Zukauskaite, J. Birch, H. Arwin, L. Hultman, *Appl. Phys. Lett.* **2010**, *97*, 112902.
[22] M. Park, Z. Hao, R. Dargis, A. Clark, A. Ansari, *J. Microelectromech. Syst.* **2020**, *29*, 490.
[23] S. Fichtner, T. Reimer, S. Chemnitz, F. Lofink, B. Wagner, *APL Mater.* **2015**, *3*, 116102.
[24] S. Fichtner, N. Wolff, G. Krishnamurthy, A. Petraru, S. Bohse, F. Lofink, S. Chemnitz, H. Kohlstedt, L. Kienle, B. Wagner, *J. Appl. Phys.* **2017**, *122*, 035301.
[25] S. Fichtner, G. Schönweger, T.-N. Kreutzer, A. Petraru, H. Kohlstedt, F. Lofink, and B. Wagner, in *Proc. 2020 IEEE ISAF*, IEEE, Keystone, CO, USA **2020**.
[26] R. Meyer, R. Waser, K. Prume, T. Schmitz, S. Tiedke, *Appl. Phys. Lett.* **2005**, *86*, 142907.
[27] H. F. Kay, J. W. Dunn, *Philos. Mag.* **1962**, *7*, 2027.
[28] M. Dawber, K. M. Rabe, J. F. Scott, *Rev. Mod. Phys.* **2005**, *77*, 1083.
[29] J. Y. Jo, Y. S. Kim, T. W. Noh, J.-G. Yoon, T. K. Song, *Appl. Phys. Lett.* **2006**, *89*, 232909.
[30] N. Ogata, M. Nagata, K. Ishihara, H. Urashima, A. Okutoh, S. Yamazaki, S. Mitarai, J. Kudo, *Jpn. J. Appl. Phys.* **1998**, *37*, 3481.
[31] K. Hironaka, C. Isobe, B. ki Moon, S. Hishikawa, *Jpn. J. Appl. Phys.* **2001**, *40*, 680.
[32] T. Kijima, H. Ishiwara, *Jpn. J. Appl. Phys.* **2002**, *41*, L716.
[33] S. Migita, H. Ota, H. Yamada, K. Shibuya, A. Sawa, A. Toriumi, T. Kijima, H. Ishiwara, *Jpn. J. Appl. Phys.* **2002**, L716. 2018, *57*, 04FB01.
[34] S. K. Ryoo, K. D. Kim, H. W. Park, Y. B. Lee, S. H. Lee, I. S. Lee, S. Byun, D. Shim, J. H. Lee, H. Kim, Y. H. Jang, M. H. Park, C. S. Hwang, *Adv. Electron. Mater.* **2022**, 2200726.
[35] A. K. Tagantsev, I. A. Stolichnov, *Appl. Phys. Lett.* **1999**, *74*, 1326.
[36] S. Oh, H. Kim, A. Kashir, H. Hwang, *Appl. Phys. Lett.* **2020**, *117*, 252906.
[37] C. Zhou, D. M. Newns, *J. Appl. Phys.* **1997**, *82*, 3081.
[38] M. Stengel, N. A. Spaldin, *Nature* **2006**, *443*, 679.
[39] J.-E. Lim, D.-Y. Park, J. K. Jeong, G. Darlinski, H. J. Kim, C. S. Hwang, S.-H. Kim, C.-Y. Koo, H.-J. Woo, D.-S. Lee, J. Ha, *Appl. Phys. Lett.* **2002**, *81*, 3224.
[40] X. Castel, M. Guilloux-Viry, A. Perrin, J. Lesueur, F. Lalu, *J. Cryst. Growth* **1998**, *187*, 211.


© 2022 The Authors. physica status solidi (RRL) Rapid Research Letters published by Wiley-VCH GmbH

18626270, 2023, 1, Downloaded from https://onlinelibrary.wiley.com/doi/10.1002/pssr.202200312 by Readcube (Labtiva Inc.), Wiley Online Library on [05/07/2023]. See the Terms and Conditions (https://onlinelibrary.wiley.com/terms-and-conditions) on Wiley Online Library for rules of use; OA articles are governed by the applicable Creative Commons License